Vacancy Generation in Si During Solid–Liquid Transition Observed by Positron Annihilation Spectroscopy

Masaki Maekawa and Atsuo Kawasuso

Advanced Science Research Center, Japan Atomic Energy Agency, 1233, Watanuki, Takasaki, Gunma 370-1292, Japan

Received December 4, 2008; accepted January 18, 2009; published online March 5, 2009

The Doppler broadening of annihilation radiation (DBAR) measurements were performed on Czochralski and floating-zone-grown Si crystals near the melting point using a positron microbeam. Below 1380 °C, the DBAR spectra showed essentially no change. In a very narrow temperature range near the melting point, the peak intensities of the DBAR spectra (*S* parameter) decreased by approximately 1% suggesting an increase in material density. Upon further heating, the *S* parameter markedly increased until melting. This indicates the formation of thermal vacancies. Compared with theoretical calculation, both monovacancies and divacancies are considered to be formed.

DOI: 10.1143/JJAP.48.030203

The diameter of current commercial Si crystals grown by the Czochralski (CZ) method exceeds 300 mm. Such an achievement in the Si industry gives us much benefit in information technology. However, the improvement of crystal quality, that is, the reduction of grown-in defects, is still a central issue in minimizing the percentage of defects in large-scale integration device fabrication.

Intrinsic defects exhausted from the molten state are frozen during the solidification. Such a process has been studied extensively through transmission electron microscopy (TEM) observation and molecular-dynamics simulations.[1–6] The formation of stacking fault tetrahedra during solidification process and the precursor state for melting were found.

Considering the large activation energy of self-diffusion (4–5 eV)[7,8] and small migration energy of single vacancies,[9] if the self-diffusion is dominated by vacancies, the thermal vacancy concentration in Si may be quite low well below the melting point. In high-temperature *in-situ* positron annihilation experiments on high-purity floating-zone (FZ) Si,[10–13] thermal vacancies have not been confirmed. Only exceptionally in heavily doped n-type Si ($\gtrsim 10^{20}\,\mathrm{cm}^{-3}$), thermal vacancies were found.[14–18]

In this study, we carried out high-temperature *in-situ* positron annihilation measurements on both CZ and FZ Si samples using a positron microbeam. The original idea is that the detection of thermal vacancies is possible by aiming the positron microbeam onto the most heated region of a sample. A precursor state for melting that is denser than solid Si was observed. Thermal vacancies were also observed near the melting point.

Samples were (i) a lightly phosphorus (P)-doped CZ Si with a resistivity in the 10–100 Ω cm range, (ii) a lightly P-doped FZ Si with a resistivity in the 10–100 Ω cm range, and (iii) a heavily antimony (Sb)-doped CZ Si with a resistivity of 0.02 Ω cm. The sample dimensions were $8 \times 1 \times 0.5$ mm^3. These samples were installed into a vacuum chamber equipped with a positron microbeam apparatus.[19] The samples were heated by passing electric current directly. Considering the Joule's heat and heat radiation, the sample temperature is empirically well-approximated by a linear equation of square root of electric power. This sample temperature was compared with that monitored using a calibrated pyrometer in a broad temperature range. Their difference was less than 5 K. Thus, in this study, sample temperature was roughly measured using the pyrometer and interpolated using the above empirical equation. A positron microbeam with an energy of 20 keV was irradiated onto the center of the sample. The Doppler broadening of annihilation radiation (DBAR) was measured as a function of temperature using a high-purity germanium detector. The typical signal-to-noise ratio of a DBAR spectrum was approximately 10^3. In one spectrum, more than 5×10^5 events were accumulated. To monitor the production of vacancies and/or any physical changes of a sample, the so-called *S* parameter, which is defined as the central area intensity of a DBAR spectrum, was determined. Here, the energy window for the *S* parameter was ±0.76 keV. The reproducibility of experiments was confirmed by repeating the same run more than two times.

To interpret the obtained Doppler broadening spectra, electron–positron momentum distribution [$\rho(\mathbf{p})$] was calculated within the local density approximation.[20–22] The valence electron wavefunctions were calculated on the basis of the norm-conserving pseudo-potential method using the ABINIT 4.1.4 code.[23] The valence electron configuration was $3s^2 3p^2$. The cut off energy of the plane-wave basis set was 30 Ry. The core electron wavefunctions were represented by the Slater function parameterized by Clementi and Roetti.[24] A self-consistent positron wavefunction was calculated on the basis of the two-component density functional theory. The Boroński–Nieminen enhancement factor was adopted.[25] The DBAR spectra $N(p)$ were obtained by convoluting $\rho(\mathbf{p})$ with the Gaussian resolution function having a half width of $5.49 \times 10^{-3} m_0 c$. Since even at the melting point the thermal energy of positron is 150 meV at most, the effect of temperature on $\rho(\mathbf{p})$ may be very small. Hence, no temperature effects were considered in the calculation.

Figure 1 shows the *S* parameter as a function of temperature. The effect of volume expansion ($10^{-5}\,\mathrm{K}^{-1}$) is smaller than the present experimental uncertainties. No distinct changes in the *S* parameter exceeding the volume expansion are seen for all types of samples up to 1380 °C. This result is consistent with that obtained in previous works.[12,13] Thus, no vacancy formation is confirmed below 1380 °C.

In the cases of lightly P-doped CZ and FZ Si samples, the *S* parameter once slightly decreases by approximately 1% at about 1407 °C and increases again upon further heating

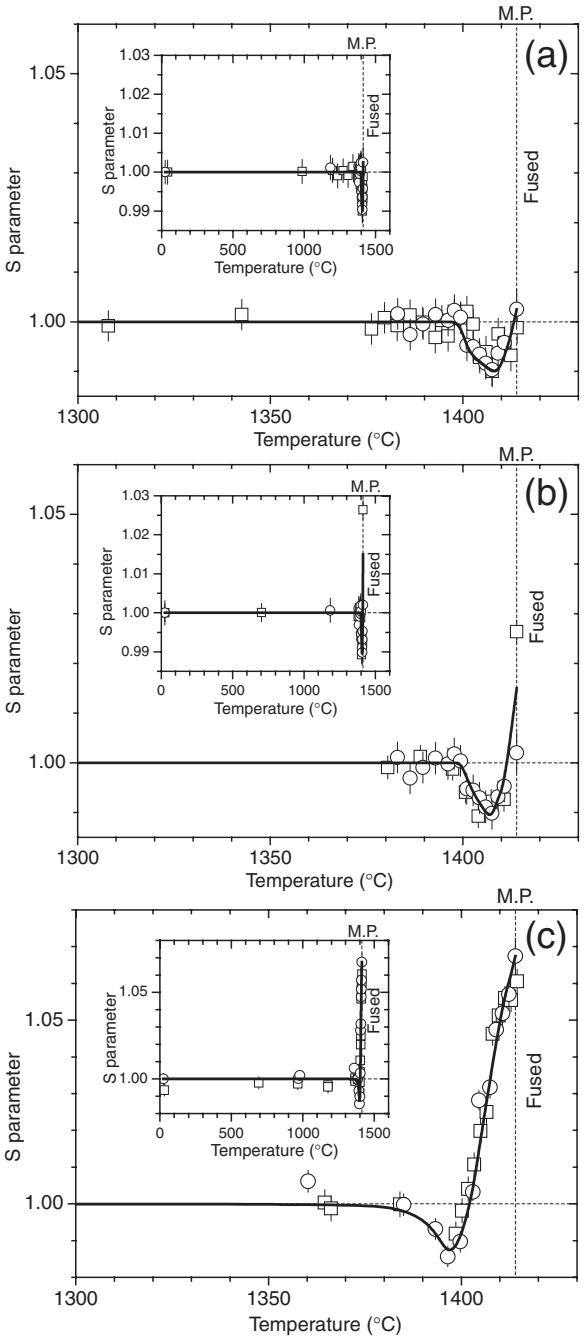

Fig. 1. *S* parameter as a function of temperature obtained from (a) lightly P-doped FZ Si, (b) lightly P-doped CZ Si, and (c) heavily Sb-doped CZ Si. Circles and squares denote the first and second heating runs, respectively. Solid lines are guides for eye.

before melting. A similar decrease in the *S* parameter is observed in the case of heavily Sb-doped CZ Si at 1398 °C, but in this case, the *S* parameter markedly increases before melting. At the end of the first heating run without melting, samples were cooled down to room temperature slowly and subsequently heated again. After cooling, the *S* parameter decreased to the original level and also, in the second heating run, the *S* parameter again changed in similarly to that in the first run.

Figure 2 shows the experimental DBAR spectrum (differentiated by that of the as-grown state) at 1407 °C, where the *S* parameter decreases, for the lightly doped FZ Si sample. Similar spectra were obtained for CZ samples. It is found

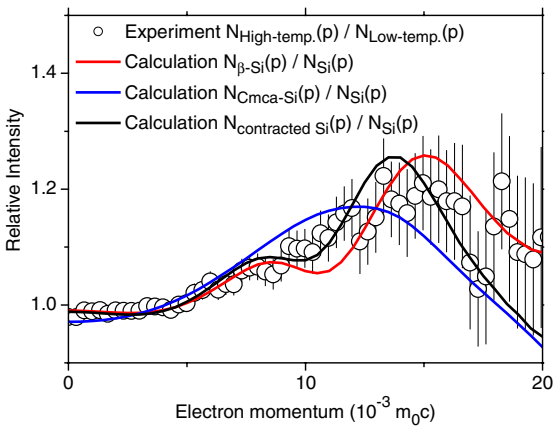

Fig. 2. (Color online) The profile indicatd by open circle denotes the DBAR spectrum at 1407 °C, where the *S* parameter decreases, obtained from the lightly P-doped FZ Si. To show differences from the as-grown state, the original spectrum was differentiated from that of the as-grown state. Red, blue, and black lines denote the DBAR spectra calculated with Si crystals of β-Sn, *Cmca*, and contracted diamond structures, respectively. All the spectra are differentiated from that calculated for Si with a diamond structure of normal lattice constant (5.43 Å).

that the DBAR spectrum becomes broader above $5 \times 10^{-3} m_0 c$. This implies the formation of some phase denser than solid Si before melting. This is ascribed to a purely bulk property since such features are observed irrespective of the doping condition and growth method. Considering the fact that after the decrease in *S* parameter the samples immediately melted, the denser phase represents the precursor state for melting. It was also found that sample resistivity started to decrease from when the *S* parameter decreased. The density of liquid Si is approximately 10% higher than that of solid Si even at zero pressure. Liquid Si exhibits a metallic conduction.[32] Therefore, the above observations may be ascribed to partial melting.

Liquid Si is thought to maintain a certain structure, similar to β-Sn and *Cmca* structures.[26–31] We thus calculated DBAR spectra assuming diamond, β-Sn, and *Cmca* structures and compared with those obtained in the experiment. In all the cases, the density is assumed to be the same for molten Si [10% heavier than solid Si (2.35 g/cm^3)]. As seen from Fig. 2, the overall feature of the experimental spectrum is in good agreement with the calculated spectra for the β-Sn and *Cmca* structures. (The amplitudes are reduced to 30 and 60%, respectively, for direct comparison.) The calculated spectra with the contracted Si only qualitatively reproduces the experiment. Thus, the decrease in the *S* parameter may be attributed to the structural transformation from diamond to β-Sn and/or *Cmca* structures.

Nishizawa *et al.* analyzed the TEM images obtained during melting in detail.[3,4] They found a transitional phase between solid and liquid phases. They further reported that the transitional phase is associated with five-member rings. The precursor state for melting found in the present study may be correlated with the transitional phase observed by TEM.

The increase in the *S* parameter above 1400 °C cannot be simply attributed to the fusion of Si. That is, the formation of thermal vacancies should be taken into account. In lightly P-doped FZ and CZ Si samples, the increase in the *S* parameter is moderated, while in heavily Sb-doped CZ Si,

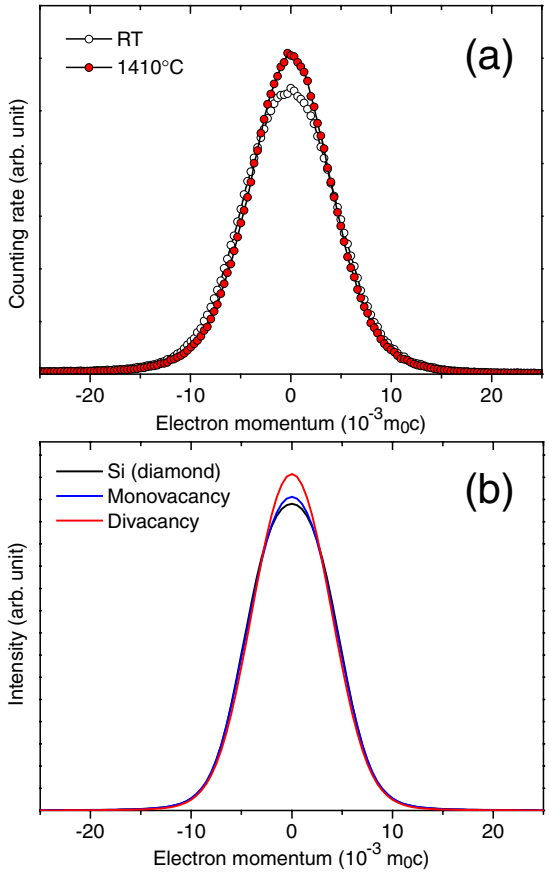

Fig. 3. (Color online) (a) Experimental DBAR spectra obtained from the heavily Sb-doped CZ Si sample in as-grown state (open circle) and at 1410 °C (red circle). (b) Calculated DBAR spectra for perfect Si (black line), monovacancy (blue line), and divacancy (red line).

the *S* parameter increases markedly. This suggests that more thermal vacancies are formed in heavily Sb-doped CZ Si. It is known that by doping impurities with larger covalent bond radii, e.g., Sn and Bi, the so-called D-defect region that is considered to originate from vacancy-type defects is well developed in CZ Si. Hence, excess vacancies may be readily formed owing to doping of oversize impurities.

Figure 3(a) shows the DBAR specra obtained from the heavily Sb-doped CZ Si sample at room temperature and 1410 °C. Figure 3(b) shows the theoretical spectra for perfect Si, monovacancy and divacancies. From this, the increase in the *S* parameter at 1410 °C is hardly explained only by monovacancy. That is, divacancies and/or further vacancy agglomerates are also formed.

Oshima *et al.* found the formation of stacking fault tetrahedra during solidification of molten Si.[1,2] This means that excess vacancies are formed in molten Si and are frozen as agglomerates. The absence of six-member rings in the transitional state also implies the introduction of vacancies. Thus, thermal vacancies are likely produced in the transitional phase near the melting point and are exhausted in the bulk region. The results obtained in the present positron annihilation experiments are consistent with those obtained by TEM studies and also the positron annihilation study of laser-irradiated Si.[34]

In summary, through positron annihilation measurements on Si using positron microbeam at high temperatures, the formation of the precursor state for melting was found. It should be a denser state than normal solid Si. After the formation of the precursor state, thermal vacancies were formed. This effect is much pronounced in heavily Sb-doped Si. Thus, thermal vacancies are formed when Si undergoes the solid–liquid phase transition.

1) R. Oshima, F. Hori, M. Komatsu, and H. Mori: Jpn. J. Appl. Phys. **37** (1998) L1430.
2) R. Oshima, F. Hori, M. Komatsu, H. Mori, T. Kamino, and Y. Yaguchi: Proc. 3rd Symp. Atomic-Scale Surface and Interface Dynamics, 1999, p. 229.
3) H. Nishizawa, F. Hori, and R. Oshima: J. Cryst. Growth **236** (2002) 51.
4) H. Nishizawa, F. Hori, and R. Oshima: Jpn. J. Appl. Phys. **42** (2003) 2805.
5) T. Motooka, K. Nishihara, R. Oshima, H. Nishizawa, and F. Hori: Phys. Rev. B **65** (2002) 081304(R).
6) K. Nishihara and T. Motooka: Phys. Rev. B **66** (2002) 233310.
7) R. F. Peart: Phys. Status Solidi **15** (1966) K119.
8) H. J. Mayer, M. Mehrer, and K. Maier: Inst. Phys. Conf. Ser. **31** (1977) 186.
9) G. D. Watkins, J. R. Troxell, and A. P. Chatterjee: Inst. Phys. Conf. Ser. **46** (1979) 16.
10) S. Dannefaer, P. Mascher, and D. Kerr: Phys. Rev. Lett. **56** (1986) 2195.
11) R. Würschum, W. Bauer, K. Maier, A. Seeger, and H. E. Schaefer: J. Phys.: Condens. Matter **1** (1989) SA33.
12) J. Throwe, T. C. Leung, B. Nielsen, H. Huomo, and K. G. Lynn: Phys. Rev. B **40** (1989) 12037.
13) A. Uedono, M. Watanabe, S. Takasu, T. Sabato, and S. Tanigawa: J. Phys.: Condens. Matter **12** (2000) 719.
14) V. Ranki, J. Nissilä, and K. Saarinen: Phys. Rev. Lett. **88** (2002) 105506.
15) V. Ranki, K. Saarinen, J. Fage-Pedersen, J. L. Hansen, and A. N. Larsen: Phys. Rev. B **67** (2003) 041201.
16) V. Ranki and K. Saarinen: Phys. Rev. Lett. **93** (2004) 255502.
17) M. Rummukainen, I. Makkonen, V. Ranki, M. J. Puska, K. Saarinen, and H.-J. L. Gossmann: Phys. Rev. Lett. **94** (2005) 165501.
18) K. Kuitunen, K. Saarinen, and F. Tuomisto: Phys. Rev. B **75** (2007) 045210.
19) M. Maekawa and A. Kawasuso: Appl. Surf. Sci. **255** (2008) 39.
20) M. J. Puska and R. M. Nieminen: Rev. Mod. Phys. **66** (1994) 841.
21) M. Alatalo, B. Barbiellini, M. Hakala, H. Kauppinen, T. Korhonen, M. Puska, K. Saarinen, P. Hautojärvi, and R. M. Nieminen: Phys. Rev. B **54** (1996) 2397.
22) A. Kawasuso, M. Yoshikawa, H. Itoh, T. Chiba, T. Higuchi, K. Betsuyaku, F. Redman, and R. Krause-Rehberg: Phys. Rev. B **72** (2005) 045204.
23) X. Gonze, J.-M. Beuken, R. Caracas, F. Detraux, M. Fuchs, G.-M. Rignanese, L. Sindic, M. Verstraete, G. Zerah, F. Jollet, M. Torrent, A. Roy, M. Mikami, Ph. Ghosez, J.-Y. Raty, and D. C. Allan: Comput. Mater. Sci. **25** (2002) 478.
24) E. Clementi and C. Roetti: At. Data Nucl. Data Tables **14** (1974) 177.
25) E. Boroński and R. M. Nieminen: Phys. Rev. B **34** (1986) 3820.
26) V. Petkov, S. Takeda, Y. Waseda, and K. Sugiyama: J. Non-Cryst. Solids **168** (1994) 97.
27) V. Petkov and G. Yunchov: J. Phys.: Condens. Matter **6** (1994) 10885.
28) V. Petkov: J. Phys.: Condens. Matter **7** (1995) 5745.
29) M. Ekman, K. Persson, and G. Grimvall: Phys. Rev. B **62** (2000) 14784.
30) Y. Waseda, K. Sugiyama, and S. Takeda: Jpn. J. Appl. Phys. **34** (1995) 4124.
31) Y. Waseda: Jpn. J. Appl. Phys. **34** (1995) 4889.
32) V. M. Glasov and S. N. Chizhevskaya: *Liquid Semiconductors* (Plenum, New York, 1969).
33) F. P. Bundy: J. Chem. Phys. **41** (1964) 3809.
34) A. La Manga, V. Privitera, G. Furtunato, M. Cuscuná, B. G. Svensson, E. Monakhov, K. Kuitunen, J. Slotte, and F. Ttuomisto: Phys. Rev. B **75** (2007) 235201.